Wind and Structures, *Vol. 28, No. 2 (2019) 129-140*
DOI: https://doi.org/10.12989/was.2019.28.2.129

Spatial correlation-based WRF observation-nudging approach in simulating regional wind field

Hehe Ren[1.2.3], Shujin Laima[1.2.3], Wen-Li Chen[1.2.3], Anxin Guo[1.2.3] and Hui Li[*1,2,3]

[1]*Key Lab of Smart Prevention and Mitigation for Civil Engineering Disasters of the Ministry of Industry and Information, Harbin Institute of Technology, Harbin, 150090, China*
[2]*Key Lab of Structures Dynamic Behavior and Control of the Ministry of Education, Harbin Institute of Technology, Harbin, 150090, China*
[3]*School of Civil Engineering, Harbin Institute of Technology, Harbin, 150090, China*

(Received February 5, 2018, Revised May 14, 2018, Accepted May 24, 2018)

Abstract. Accurately simulating the wind field of large-scale region, for instant urban areas, the locations of large span bridges, wind farms and so on, is very difficult, due to the complicated terrains or land surfaces. Currently, the regional wind field can be simulated through the combination of observation data and numerical model using observation-nudging in the Weather Research and Forecasting model (WRF). However, the main drawback of original observation-nudging method in WRF is the effects of observation on the surrounding field is fully mathematical express in terms of temporal and spatial, and it ignores the effects of terrain, wind direction and atmospheric circulation, while these are physically unreasonable for the turbulence. For these reasons, a spatial correlation-based observation-nudging method, which can take account the influence of complicated terrain, is proposed in the paper. The validation and comparation results show that proposed method can obtain more reasonable and accurate result than original observation-nudging method. Finally, the discussion of wind field along bridge span obtained from the simulation with spatial correlation-based observation-nudging method was carried out.

Keywords: wind field; complex terrain; spatial correlation-based WRF observation-nudging method; long-span bridges; wind heterogeneous distribution character; local wind environment

1. Introduction

The wind field under land surface pattern of complex terrain or urban community is extremely complicated. With the increasing computational power, numerical model as a research tool to simulate the urban wind environment becomes possible and developments quickly (Bitsuamlak and Abdi 2016, Shen *et al*. 2017, Liu *et al.* 2017). For obtaining the accurate and reasonable wind field, it is necessary to adopt appropriate inflow and boundary conditions. The observation data measured at meteorological station is usually as the inflow and boundary conditions (Liu *et al.* 2017). Because complex terrain and urban environment is related to multiscale geometric sizes, the WRF is a good choice for simulating continuous multiscale wind field. Also, WRF takes account the multi-physics process (wind, temperature, humidity, water vapor, etc.) to simulate the wind field under natural atmosphere and terrain, then the simulation result could be used as the inflow and boundary conditions of computational fluid dynamics (CFD) (Liu *et al.* 2011, Zajaczkowski *et al.* 2011, Cheng *et al*. 2015). The following focuses on numerical model WRF and observation-nudging method in WRF.

WRF is a state-of-the-art atmospheric modeling system designed for both meteorological research and numerical weather prediction. It offers a host of options for atmospheric processes and can run on a variety of computing platforms. WRF excels in a broad range of applications across scales ranging from tens of meters to thousands of kilometers (Skamarock *et al.* 2008). The simulation results can be used to evaluate the wind potential of the simulated area in a methodological point of view (Monti *et al*. 2017), which corresponding the view of microscale (Dhunny *et al*. 2015, Weerasuriya *et al*. 2016, Li *et al*. 2016), and can be used as the inflow condition of CFD simulation (Cheng *et al*. 2015).

However, the initial and boundary conditions in WRF are relative rough, and the simulation result of local wind field is not accurate and refined enough. To get more accurate local wind field, four-dimensional data assimilation (FDDA) and variational data assimilation are usually employed in the current WRF version 3.7.1 to guide the simulation, which can combine the advantages of both WRF model and observations simultaneously. Considering the observations on the mesoscale are sometimes sparse and typically are not very uniformly distributed in space, the observation-nudging method (Liu *et al.* 2005) is a good choice. The method allows the model to effectively assimilate temperature, wind and moisture observations from all platforms, measured data at any location within the model domains and any time within a given data assimilation periods with the observation-nudging formulation. The observation-nudging method is a continuous data simulation method that relaxes the model state toward the observed state by adding one or more

*Corresponding author, Professor
E-mail: lihui@hit.edu.cn

ISSN: 1226-6116 (Print), 1598-6225 (Online)

artificial tendency terms of the prognostic equations based on the difference between the two states. Observation-nudging directly toward individual observations distributed nonuniformly in space and time, it uses only those observations that fall within a predetermined time window centered about the current model time step. And the set of differences between the model and the observed state is computed at the observation locations. These "corrections" with proper space and time weights are then analyzed back to the grid according to the model dynamics within a region surrounding the observations (Liu *et al.* 2008).

Stauffer and Seaman (1994) showed that nudging toward observations was more successful on the mesoscale than nudging toward analyses. Seaman *et al.* (1995) focused on objective validation of the regional mesoalpha-scale results, it has been shown that a multiscale data assimilation approach can produce highly reliable simulations of the wind, temperature, mixed layer depth and moisture. Fast (1995) showed that the current data assimilation technique can have a positive impact on the mesoscale flow fields, however, care must be taken in its application to grids of relatively fine horizontal resolution. Leslie *et al.* (1998) found that the impact of observation-nudging same as 4D variational technique assimilates the same data, the difference is that the former was practicable while the latter was too large computational cost.

Also, some applications of Newtonian relaxation method used in nudging approach are concluded. Davis *et al.* (1999) focused on mesoscale predictability over complex terrain and heterogenous land surfaces. Rife *et al.* (2002, 2004) studied the diurnal boundary layer circulations in the Great Basin Desert and the predictability of low-level winds over the Salt Lake valley and surrounding mountains, respectively. Warner *et al.* (2004) studied on emergency-response applications of high-resolution mesoscale simulations through graphical interfaces. Liu *et al.* (2006a, 2006b) validated the Newtonian relaxation method for the Oklahoma City area during the Joint Urban 2003 Field Project show quite satisfactory performance of the model system in resolving the observed surface variables and mesoscale circulation associated with an urban environment. Pan *et al.* (2011) studied the influence of climate change to California and Nevada regions by high-resolution dynamical downscaling model. Zhang *et al.* (2016) studied on the impacts of assimilating the TAMDAR data in 12/4 km grid WRF-Based RTFDDA simulations over the CONUS.

When assigning the weight of an observation to the nudging term at each grid point, the horizontal-influence functions are constructed to account for blocking effect of elevated terrain. For each grid point, the terrain-elevation difference between the grid point and observation stations is calculated, and if this is larger than a specific amount the observation will not be allowed to affect the grid point. This is especially important because most of the grids of the forecast models have complex orography. In Xu *et al.* (2002) the specific value is 500 m, that is, if there is a terrain blockage or a valley depth larger than 500 m, the nudging weight for the observation at the given grid point is set to zero, then the terrain-adjusted nudging weights are shown to produce certain reasonable effects in the final analysis and slightly improved verification statistics.

Even through Xu *et al.* (2002) considered the terrain effects, the result is not improved so much, especially for complex terrain. Two reasons here can be concluded. First, too simple to consider the terrain effect, just use a step function to define the effects of terrain, and why the specific value is 500 m which is not clear. Second, the model of the temporal and spatial weighting function in observation-nudging method is still mathematical meaning, rather than physical meaning. And for the study of wind field at the scale of civil engineering, it is necessary to consider the wind field around the monomer structure, at this case the refine local terrain will have a great influence on wind field. Therefore, we propose a spatial correlation-based observation-nudging method based on physics, which considers the effects of terrain, wind direction, atmospheric circulation and so on, especially for complex terrain and land surface of urban community cases.

2. Spatial correlation-based WRF observation-nudging approach

The mesoscale numerical model WRF can take account the multi-physics process (wind, temperature, humidity, water vapor, etc.) to simulate the wind field under real atmosphere and terrain. The advantages of WRF model are multi-physics and can obtain the local spatial wind field, while the disadvantage is that the simulation result of wind velocity has a certain deviation from observation data. In contrast, the advantage of the observation data is of high reliability, while the number of observation locations is very limited. If the advantages of WRF model and observation data are combined, the simulated wind field can be improved with more accuracy.

The observation-nudging module in WRF has the function of implement the combination of observations and mesoscale numerical model. However, the main drawback of original observation-nudging method in WRF is that the effects of the observation on the surrounding field is fully mathematical express in terms of temporal and spatial domains. In addition, it ignores the effects of terrain, wind direction and atmospheric circulation, while these are physically unreasonable. For these reasons, a spatial correlation-based observation-nudging method is proposed in this paper and the influence of above factors can be taken account. The WRF mesoscale numerical model, the original and proposed spatial correlation-based observation-nudging methods will be described in following subsection here, respectively.

2.1 Original WRF observation-nudging approach

The WRF model is a fully compressible and nonhydrostatic model, wherein the vertical coordinate is a terrain-following hydrostatic pressure coordinate, and the staggering grid is Arakawa C-grid. 2 or 3 order Runge-Kutta algorithm in time integration, and 2 to 6 order advection schemes in both the horizontal and vertical

directions are employed in the model. A time-split small step for acoustic and gravity-wave modes is used. The detailed description of the WRF can be referred to NCAR technical note (Skamarock *et al.* 2008). The governing equations are written as follows

$$\partial_t U + m_x[\partial_x(Uu) + \partial_y(Vu)] + \partial_\eta(\Omega u) + (m_x / m_y)[\mu_d \alpha \partial_x p + (\alpha / \alpha_d \partial_\eta p \partial_x \phi)] = F_U \quad (1)$$

$$\partial_t V + m_y[\partial_x(Uv) + \partial_y(Vv)] + (m_y / m_x)\partial_\eta(\Omega v) + (m_y / m_x)[\mu_d \alpha \partial_y p + (\alpha / \alpha_d \partial_\eta p \partial_y \phi)] = F_V \quad (2)$$

$$\partial_t W + m_x[\partial_x(Uw) + \partial_y(Vw)] + \partial_\eta(\Omega w) - m_y^{-1} g[(\alpha / \alpha_d)\partial_\eta p - \mu_d] = F_W \quad (3)$$

$$\partial_t \mu_d + m_x m_y[\partial_x U + \partial_y U] + m_y \partial_\eta(\Omega) = 0 \quad (4)$$

$$\partial_t \Theta + m_x m_y[\partial_x(U\theta) + \partial_y(V\theta)] + m_y \partial_\eta(\Omega\theta) = F_\Theta \quad (5)$$

$$\partial_t Q_m + m_x m_y[\partial_x(Uq_m) + \partial_y(Vq_m)] + m_y \partial_\eta(\Omega q_m) = F_{Q_m} \quad (6)$$

$$\partial_t \phi + \mu_d^{-1}[m_x m_y(U\partial_x \phi + V\partial_y \phi) + m_y \Omega \partial_\eta \phi - m_y g W] = 0 \quad (7)$$

$$\eta = (p_h - p_{ht}) / \mu \qquad \mu = p_{hs} - p_{ht} \quad (8)$$

where, Eqs. (1)-(3) are the momentum equations; Eq. (4) is the mass conservation equation; Eqs. (5) and (6) are the conservation equations for the potential temperature and scalars; Eq. (7) is the geopotential equation. x, y and η denote the longitudinal, latitudinal and terrain-following hydrostatic-pressure vertical coordinates, respectively, and U, V and W denote the longitudinal, latitudinal and terrain-following hydrostatic-pressure vertical velocity components, respectively. p_h is the hydrostatic component of the pressure, p_{hs} and p_{ht} are the subcomponents along the surface (bottom) and top boundaries, respectively. $\mu(x,y)$ and μ_d represent the mass per unit area and the mass of the dry air within the column in the model at (x,y), respectively. $\vec{V} = \mu\vec{v} = (U,V,W)$, $\Omega = \mu\dot{\eta}$, $\Theta = \mu\theta$ are the appropriate flux form variables of velocity in the coordinate (x,y,z), the vertical velocity in the coordinate (x,y,η), the potential temperature, and $\vec{v} = (u,v,w)$ are the covariant velocities in the two horizontal and vertical directions, respectively, while $\dot{\eta}$ is the contravariant 'vertical' velocity. θ is the potential temperature, indicating a parcel of fluid at pressure p is the temperature that the parcel can be attained if the parcel of fluid is adiabatically brought to a standard reference pressure p_0 (1000 millibars). The non-conserved variables $\phi = gz$ is the geopotential, p is the pressure, α_d is the inverse density of the dry air $(1/\rho_d)$ and α is the inverse density taking into account the full parcel density $\alpha = \alpha_d(1 + q_v + q_c + q_r + q_i + ...)^{-1}$, $q_m = q_{v,} q_{c,} q_{r,} q_{i,} ...$, q_m is the mass mixing ratio of water vapor, cloud, rain, and ice with respect to the dry air. $Q_m = \mu_d q_m$ is the appropriate flux form of the mass mixing ratio of water vapor, cloud, rain and ice with respect to the dry air. $\partial_t U$, $\partial_t V$ and $\partial_t W$ are the derivatives with respect to time, $\partial_x U$ and $\partial_y U$ are the gradient of two horizontal velocities, respectively. In the WRF's computational space, the grid distances of longitudinal and latitudinal $(\Delta x, \Delta y)$ are constants. Orthogonal projects to the sphere require that the physical distances between grid points in the projection vary with position on the grid. To transform the governing equations, map scale factors m_x and m_y are defined as the ratio of the distance of horizontal grid points in computational space to the corresponding distance on the earth's surface: $(m_x, m_y) = (\Delta x, \Delta y) /$ (distance on the earth). The right-hand side terms in these equations include the Coriolis terms, mixing terms and parameterized physics.

Since the WRF simulation results are not accurate enough, it is expected to incorporate the observation data to correct the WRF simulation, which enables to get more accurate wind field. Observation-nudging is a form of Newtonian relaxation wherein artificial tendency terms are implemented into the model to gradually "nudge" the model towards observations. These nudging terms synchronize the model atmospheric states at each grid point towards the observations in proportion to the differences between the model solutions and observations. Each observation affects the model states in proportion to the temporal and spatial weights that are maximized at its observed time and location, and the model spreads the observed information in time and space according to the model dynamics. In fact, based on the principles of relaxation method, it is well understood observation-nudging method working in this way: assuming the target value F^* has two accompanying approximations F_0 (WRF model result) and F_1 (observation data), in order to obtain higher precision result, take weighted average of the two approximations as the transformation value, appropriate selection of the weight coefficient to adjust the extent of correction, this is well known as relaxation technology because of this adjustment based on the extent of correlation and loose, that is

$$F^* = (1-\omega)F_0 + \omega F_1 = F_0 + \omega(F_1 - F_0) \quad (9)$$

Assuming the observation data is the correct solution of the WRF governing equation, the observation-nudging governing equation can be obtained by similar theory as follows

$$\frac{\partial a_{obs}}{\partial t} = F_a \quad (10)$$

$$\frac{\partial a_{wrf}(x_i, y_i, z_i, n+1)}{\partial t} = F_a(x_i, y_i, z_i, n) + \frac{\partial(a_{wrf}(x_i, y_i, z_i, n) - a_{obs}(x_i, y_i, z_i, n+1))}{\partial t} \quad (11)$$

$$\frac{\partial a\mu}{\partial t}(x_i,y_i,z_i,n+1)=F_a(x_i,y_i,z_i,n)+\mu G_a\frac{\sum_{j=1}^{N}W_a^{\,2}(x_j,y_j,z_j,n+1)[a_{wrf}(x_i,y_i,z_i,n)-a_{obs}(x_i,y_i,z_i,n+1)]}{\sum_{j=1}^{N}W_a(x_j,y_j,z_j,n+1)} \quad (12)$$

$$w_{xy}=\begin{cases}\dfrac{R_H^{\,2}-D^2}{R_H^{\,2}+D^2} & \begin{cases}0\le D\le R_H\\ D>R_H\end{cases}\\ 0\end{cases} \quad (13)$$

$$w_z=\begin{cases}1-\dfrac{|p_{ob}-p|}{R_z} & \begin{cases}|p_{ob}-p|\le R_z\\ |p_{ob}-p|>R_z\end{cases}\\ 0\end{cases} \quad (14)$$

$$w_t=\begin{cases}1 & \\ \dfrac{\tau-|t-t_{ob}|}{\tau/2} & \begin{cases}|t-t_{ob}|<\tau/2\\ \tau/2\le|t-t_{ob}|<\tau\end{cases}\\ 0 & |t-t_{ob}|>\tau\end{cases} \quad (15)$$

where, the Eq. (10) is based on observations satisfying the N-S equation; Eq. (11) is the implicit solution to the $n+1$ step of the N-S equation; then easily to get the Eq. (12), which is the implemented way of observation-nudging method in WRF. a is the quantity being nudged (e.g., u,v,θ,q, etc.), F_a represents the physical tendency terms of a (this includes advection, diffusion, etc.), G_a is the nudging strength for a, N is the total number of observations, i is the index to the current observation, a_{obs} is the observed value of a, and $a_{wrf}(x_i,y_i,z_i,n)$ is the model value of a interpolated to the observation location. The quantity $a_{wrf}-a_{obs}$ is the updated item; the updated item associated with a given observation varies with time as the model value $a_{wrf}(x_i,y_i,z_i,n)$ varies. Thus, as the model value approaches the observed value, the nudging tendency term decreases. $W_a(x,y,z,n)=w_{xy}\cdot w_z\cdot w_t$ is the spatiotemporal weighting function based on the temporal and spatial separation between the observation and the current model location; in the current WRF version 3.7.1, the horizontal weight w_{xy} is a Cressman-type weighting function that depends on the horizontal distance D between the observation and the nudging grid point, R_H is the horizontal influence radius, as shown in Eq. (13); the vertical weight w_z is in general proportional to the vertical separation between the grid point and the observation, p_{ob} and p is the pressure at observation location and grid point, respectively; R_z is the vertical influence distance (η coordinate), as shown in Eq. (14); the temporal weight w_t is defined as a function of the time window with half-width τ and designed to avoid sharp changes in the weight attached to certain observations, t is the calculation time, t_{ob} is the time that observation data is added into the WRF, as shown in Eq. (15).

The processes of observation-nudging method are as follows: according to the results of the WRF simulation, eight spatial points (cubes) around the observation location are selected for the three-linear interpolation to obtain the value of WRF simulation result at the observation location; then the tendency term of each grid point in the affected area is obtained according to the weighting factor; and finally, solve the governing equation.

2.2 Proposed Spatial correlation-based observation-nudging approach

In terms of physics, the weighting function $W(\mathbf{x},t)$ of observation-nudging method represents the influence intensity of the observations on the surrounding locations, or can be regarded as the correlation between them. From this point of view, it can be found that the weighting function in the current WRF version 3.7.1 is not reasonable for simulating the wind field with complex terrain. As shown in Eqs. (13)-(15), the weighting function of original observation-nudging approach is only the distance function, which means that the weighting function is the same for any points which have the same distance from observation point. Obviously, it is not true for the atmosphere boundary layer and the weighting function is severely affected by the terrain. As well known, the mutual influence of variables at two positions can be represented by the spatial correlation function. Therefore, to take account of the local terrain effects, the weighting function $W(\mathbf{x},t)$ is replaced by the spatial correlation function $R(\mathbf{x},t)$ of the observed local wind velocity in the study. The correlation function is expressed as follows

$$R(a(x_o,y_o,z_o),a(x_i,y_i,z_i))=\frac{Cov(a(x_o,y_o,z_o),a(x_i,y_i,z_i))}{\sqrt{Cov(a(x_o,y_o,z_o),a(x_o,y_o,z_o))Cov(a(x_i,y_i,z_i),a(x_i,y_i,z_i))}} \quad (16)$$

$$Cov(a(x_o,y_o,z_o),a(x_i,y_i,z_i))=E[(a(x_o,y_o,z_o)-E[a(x_o,y_o,z_o)])(a(x_i,y_i,z_i)-E[a(x_i,y_i,z_i)])] \quad (17)$$

where a is nudged variables (e.g., u,v,θ,q, etc.) at observation position and computational grid point, same as the variables in Eq. (12). $a(x_o,y_o,z_o)$ and $a(x_i,y_i,z_i)$ are the variable at observation position (x_o,y_o,z_o) and computational grid point (x_i,y_i,z_i), respectively. The correlation coefficient can be calculated according to the requirements of different time scales, for example, 10 min and 1 min intervals. In the following discussions, the proposed method is termed as spatial correlation-based WRF observation-nudging approach.

For obtaining the correlation function of the local wind field, the most accurate way is to use the field measurement

data. However, it is very hard and expensive to carry out the field measurement over a large range because the wind speeds at different locations should be measured simultaneously. However, for the nature wind affected by the terrain, it is well known that the coherent function of two points decays fast in the high frequency domain, which indicates that the correlation is mainly contributed by the large-scale turbulence with low frequency. Based on the fact, in the present study, an alternate way is adopted, that is the spatial correlation of the wind field obtained from the WRF without nudging method is used. Because the WRF mainly contain large-scale vortex, the precision is enough for those points with far distance. The correlation intensity may be down estimated for those points close each other because the correlation intensity is influenced dramatically by the small-scale vortex for these points. Fortunately, for the present study, the largest and smallest computational grid space is 12.150 km and 150 m, respectively, the large-scale vortex plays a key role, so the precision of spatial correlation of the wind field obtained from the WRF without nudging method is good enough.

The specific realization steps of spatial correlation-based WRF observation-nudging method are as follows: First, correlation analysis in Eq. (16) between the observation location and nudged grid points from the results of WRF without observation-nudging is carried out; then the tendency term based on the correlation coefficient in Eq. (12) is calculated; and finally, the governing equations are solved.

3. Validation

3.1 Wind field location and simulation scheme

The simulation wind field locates at longitude 116°00′~127°00′ E, latitude 24°30′~35°30′ N, five domains (Fig. 1(a)) are divided to simulate the wind field at different sizes of mesh grid (the detail shown in Table 1), we focus on the region of longitude 121°50′~122°00′ E, latitude 30°02′~30°09′ N (Domain 5) in the East China Sea, with the area of about 15 km × 15 km, and the region and topographic elevation map are shown in Fig. 1(b). Because there is an asymmetric suspension bridge with a 1650 m central span and one 578 m side span in the region (see in Fig. 2), the wind field distribution is very important for design of this bridge in this region. To monitor the free wind speeds at the bridge site, ultrasonic anemometers are installed at the 1/4, 1/2 and 3/4 central span of the bridge, which is 54.5 m above the sea surface. In the WRF observation-nudging simulation, the monitored inflow wind velocity at 1/4 central span is selected as observation data incorporated to the simulation model, while the inflow wind velocities at 1/2 and 3/4 central span are selected as validation data. From the topographic elevation map shown in Figs. 1 and 2, it can be observed that there are mountains in the left of observation locations, which dramatically influence the wind velocities. The simulation period 2014_09_22_18:00:00~2014_09_23_00:00:00 (UTC) is a segment of typhoon Fung-wong event, which is the 16th typhoon in 2014. The track of typhoon Fung-wong is shown in Fig. 3. It is noted that the bridge is not included in the simulation due to very small size to compare with the simulation region.

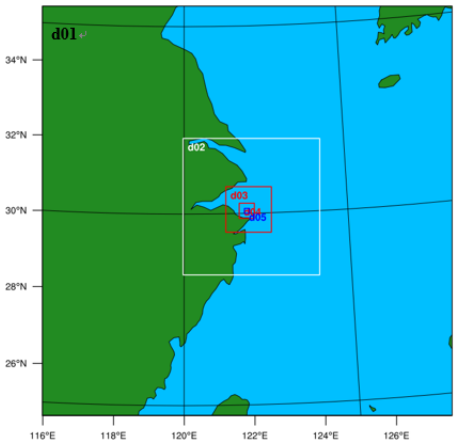

(a) Domain configuration of simulation. d01, the outermost layer of computation domain; d05, the innermost layer; d02, d03, d04 are the 2th, 3th, 4th layer, respectively

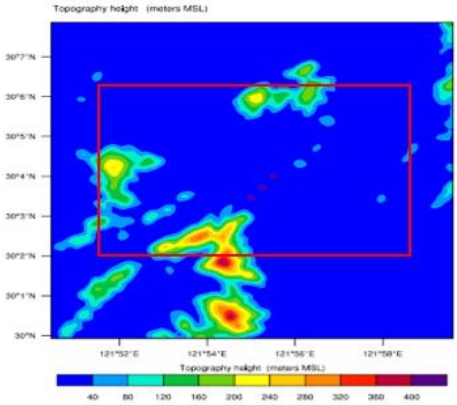

(b) Topographic elevation map of d05

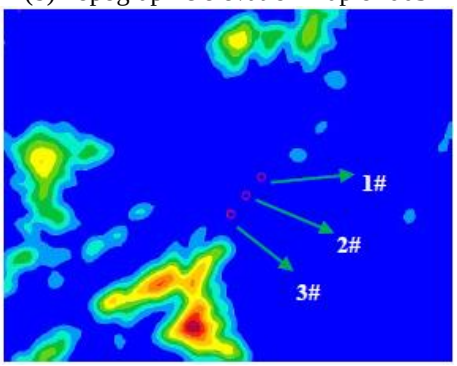

(c) An enlarged view of the red box in (b)

Fig. 1 The simulated region and observation locations. where point 1# is the observation location (1/4 central span of the bridge); point 2# and 3# are the validation locations (1/2 and 3/4 central span of the bridge, respectively)

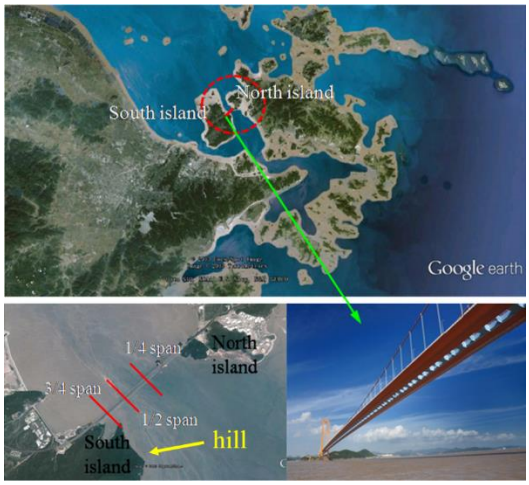

Fig. 2 Bridge site and anemometer installation locations

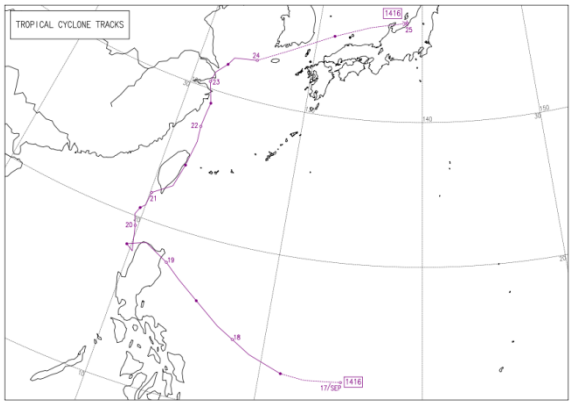

Fig. 3 The track of typhoon Fung-wong

Table 1 The basic parameters of WRF running

The simulated period	2014_09_22_18:00:00~2014_09_23_00:00:00 (UTC)				
Algorithm	WRF				WRF-LES
Domain	1	2	3	4	5
Horizontal grid distance (m)	12,150	4,050	1,050	450	150
Horizontal grid number	100 × 100	100 × 100	100 × 100	100 × 100	100 × 100
Vertical layer number	75	75	75	75	75
Time step (s)	81	27	9	3	1
Terrain, vegetation precision	5 min	2 min	30 s	3 s	2 s

To validate the advantage of the proposed spatial correlation-based WRF observation-nudging method, three simulation cases are included in the study. Case-0, WRF without nudging method; Case-1, original WRF nudging with 10min time interval observation data and 1min time window; Case-2, spatial correlation-based WRF nudging with 10min time interval observation data and 1min time window. It should be noted that, the correlation coefficient precision for original observation-nudging method is controlled by $W(\mathbf{x},t)$ in Eq. (12), while for spatial correlation-based observation-nudging method, it is controlled by correlation coefficient $R(\mathbf{x},t)$ in Eq. (16). In general, 10 min represents the mean wind characteristics in the statistical sense, but for the real atmospheric, the change of the wind field may be more frequently, which is certainly less than the 10 min interval in the case of complex terrain. Therefore, the time window is set to 1 min.

Table 2 The parameters setting of observation-nudging

Cases	description	R_H	R_z	τ	G_α	R
Case-0	WRF without nudging method	--	--	--	--	--
Case-1	Original WRF nudging with 10min time interval observation data and 1min time window	3 km	0.05	1 min	0.01667	--
Case-2	Spatial correlation-based WRF nudging with 10min time interval observation data and 1min time window	--	--	1 min	--	1min_coeff

Table 3 Information of observation and validation data

Number	Longitude	Latitude	Height
Observation point (1#)	121.9294	30.0686	54.5 m
Validation point (2#)	121.9265	30.0659	54.5 m
Validation point (3#)	121.9235	30.0632	54.5 m

For all the simulated cases, the standard parameterization schemes have been configured for the analysis region. i.e., the Yonsei University planetary boundary layer scheme (YSU) (Hong *et al.* 2006), WRF Single-Moment 5-class microphysics scheme (WSM5) (Hong *et al.* 2004), Grell-Freitas ensemble cumulus scheme (GF) (Grell and Freitas 2014), Rapid Radiative Transfer Model for longwave radiation (RRTM) (Mlawer *et al.* 1997), Rapid Radiative Transfer Model for General Circulation Models for shortwave radiation (RRTMG) (Iacono *et al.* 2008), and Unified Noah land-surface model for land soil processes (Noah) (Chen and Dudhia 2001).

The WRF running basic parameters and observation-nudging setting parameters are shown in Tables 1 and 2, respectively. In the WRF observation-nudging simulation, only the observation inflow wind velocity at 1/4 central span is incorporated to the model, while the observation inflow wind velocities at 1/2 and 3/4 central span are just selected as validation data. The detailed information of observation locations is listed in Table 3.

3.2 Validation results

The simulated average wind velocity at observation location (1#) are shown in Fig. 4. As shown in Fig. 4, the results of Case-0 (WRF without nudging) have largest error compared with observed wind velocity, in which the maximum error of average wind velocity is up to -78.05%, the average error of average wind velocity is -42.26%. With incorporation of observed data, accuracy of simulation results obtained by original WRF observation-nudging method (Case-1) has been improved. However, the errors are still large, in which the maximum error of average wind velocity is up to -54.39%, the average error of average wind velocity is -27.50%. While the results obtained by the spatial correlation-based WRF observation-nudging method (Case-2) have been further remarkably improved, wherein the maximum error of average wind velocity is -36.82%, the average error of average wind velocity is -7.13%, indicating that the method with spatial correlation has good ability to accurately simulate the local wind field. And the trend of spatial correlation-based observation-nudging method is also better than that original observation-nudging method and WRF without nudging method. The comparison of results implies that the spatial correlation-based WRF observation-nudging method has good ability if the terrain effects cannot be ignored.

To further validate the spatial correlation-based WRF observation-nudging method, the simulation results are compared with the measured velocities at another two observation locations (2# and 3#), as shown in Figs. 5 and 6, respectively. It should be noted that the observation data at these two locations are not incorporated to the WRF observation-nudging model. It can be seen from Figs. 5 and 6 that both simulated velocities agree well with the observation data.

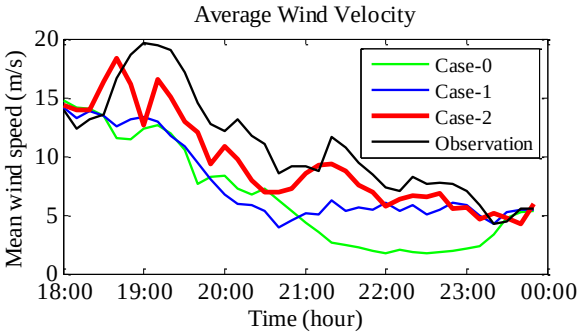

Fig. 4 Mean wind velocity at observation point (1#)

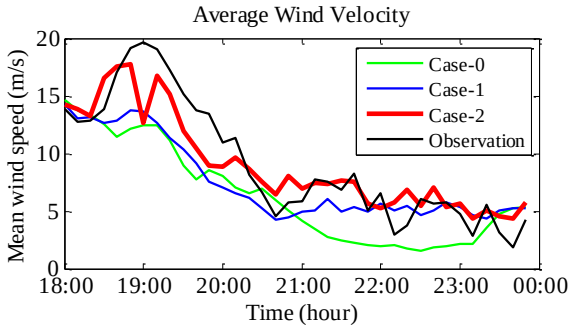

Fig. 5 Mean wind velocity at validation point (2#)

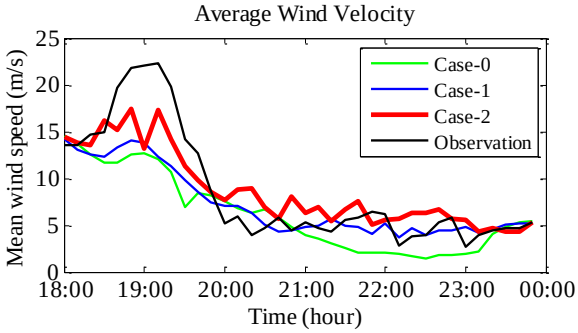

Fig. 6 Mean wind velocity at validation point (3#)

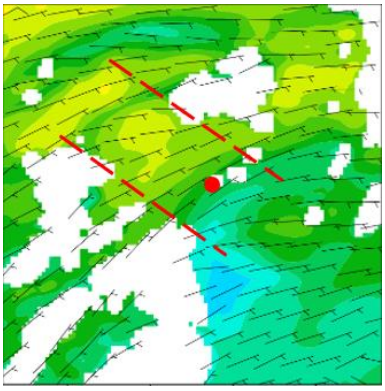

(i) Wind field during 20:40-20:50

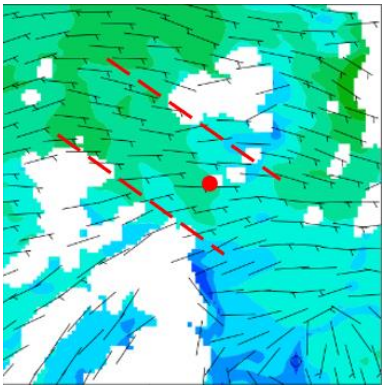

(ii) Wind field during 21:10-21:20

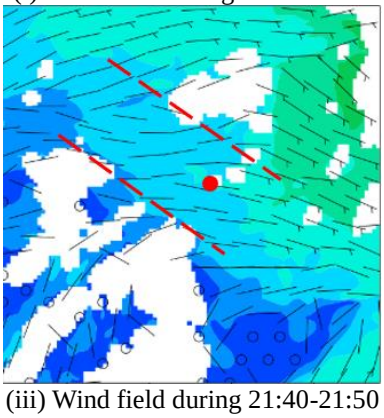

(iii) Wind field during 21:40-21:50

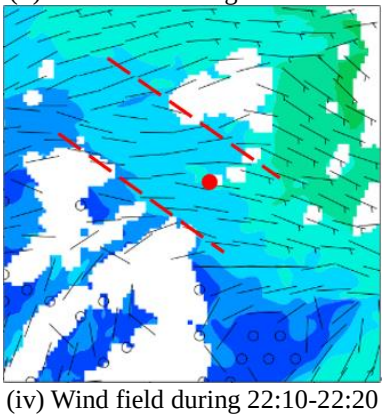

(iv) Wind field during 22:10-22:20

(a) WRF without observation-nudging method

Continued-

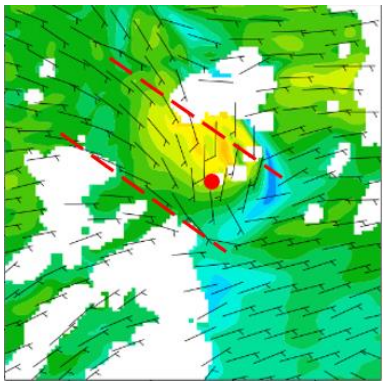

(i) Wind field during 20:40-20:50

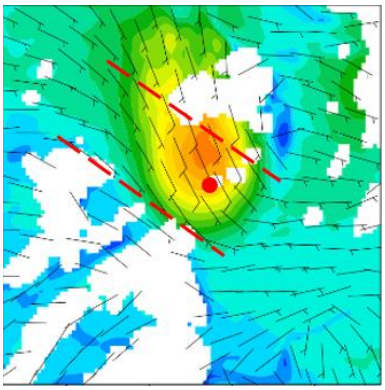

(ii) Wind field during 21:10-21:20

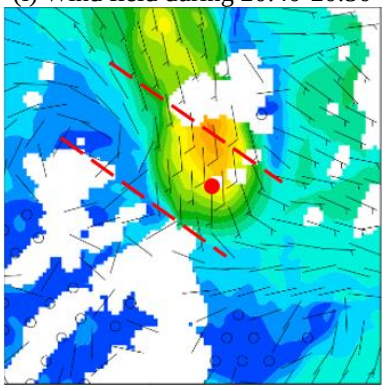

(iii) Wind field during 21:40-21:50

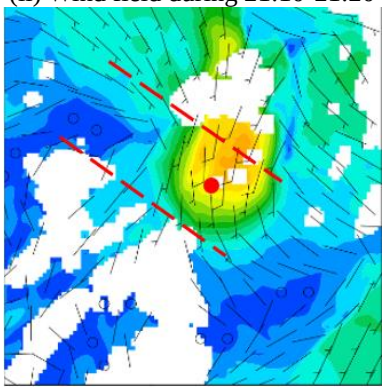

(iv) Wind field during 22:10-22:20

(b) Original WRF observation-nudging method

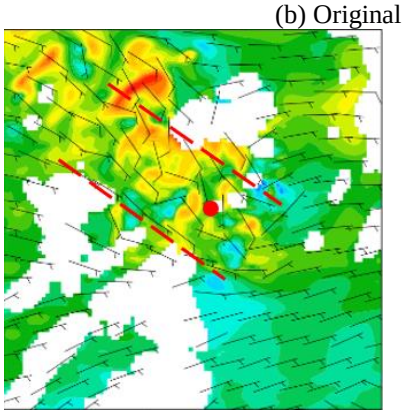

(i) Wind field during 20:40-20:50

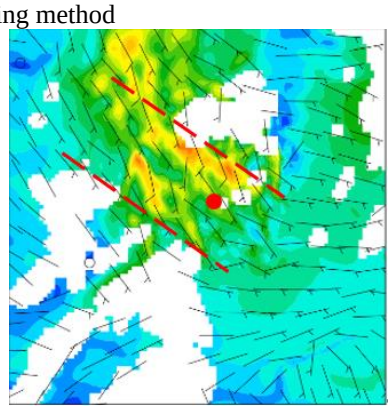

(ii) Wind field during 21:10-21:20

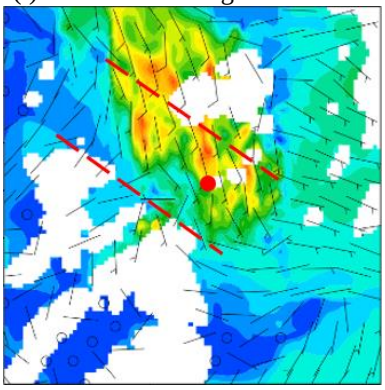

(iii) Wind field during 21:40-21:50

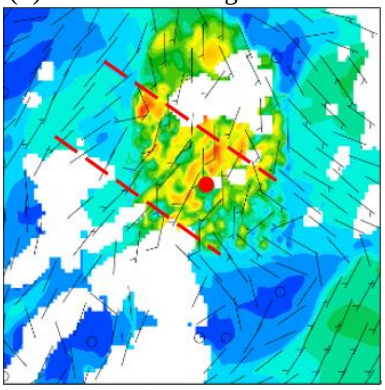

(iv) Wind field during 22:10-22:20

(c) Spatial correlation-based WRF observation-nudging method

Continued-

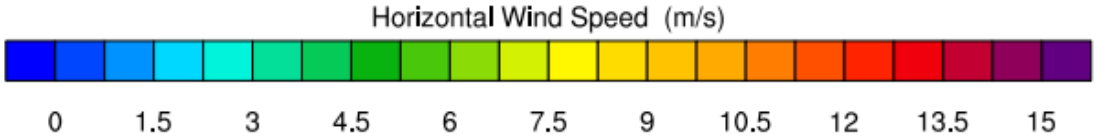

Fig. 7 The wind field obtained from WRF without nudging method, original observation-nudging method and spatial correlation-based observation-nudging method. Each subgraph from left to right are the contours of wind velocities (z = 54.5 m) at 2014_09_22_20:50:00 ~ 2014_09_22_22:20:00, the increment is 30min

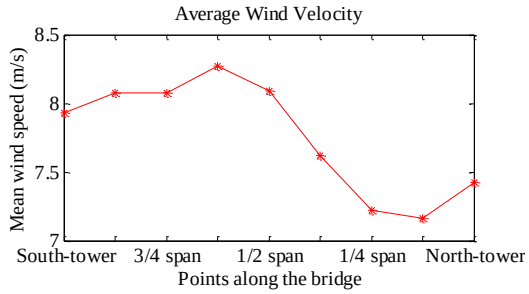

(i) Mean wind speed during 20:40-20:50

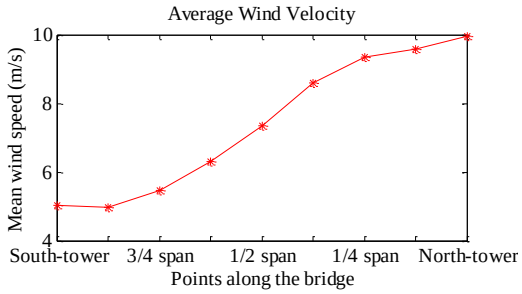

(ii) Mean wind speed during 21:10-21:20

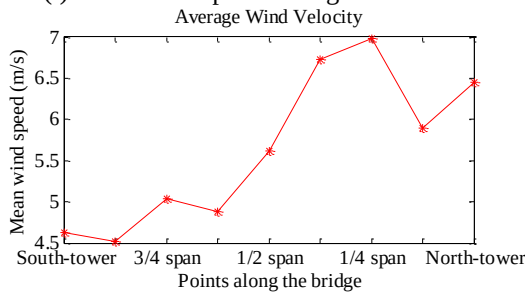

(iii) Mean wind speed during 21:40-21:50

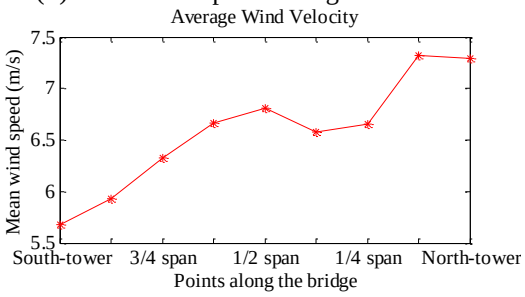

(iv) Mean wind speed during 22:10-22:20

(a) Mean wind velocity

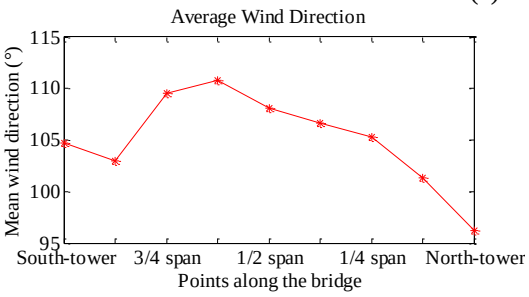

(i) Mean wind direction during 20:40-20:50

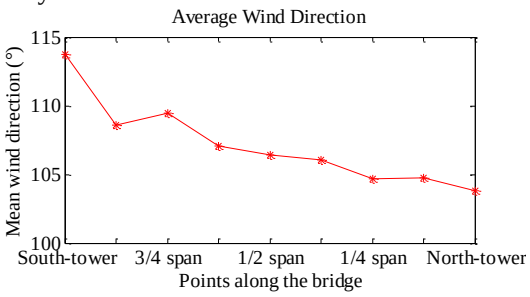

(ii) Mean wind direction during 21:10-21:20

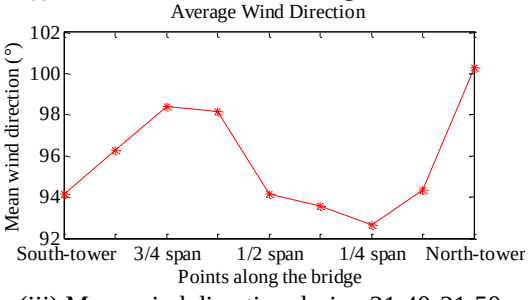

(iii) Mean wind direction during 21:40-21:50

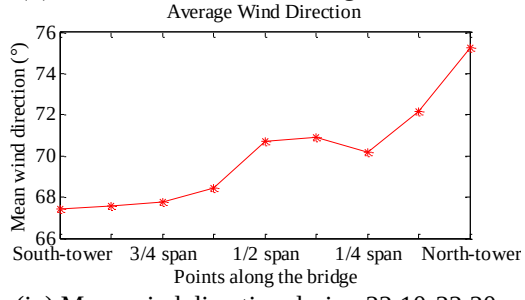

(iv) Mean wind direction during 22:10-22:20

(b) Mean wind direction

Fig. 8 The average wind characteristics of the bridge span under spatial correlation-based observation-nudging method

Based on the validation results, it can be concluded that the spatial correlation-based WRF observation-nudging approach has a good ability to accurately capture the local wind field under the terrain effects if there is observation data. In addition, the proposed method has much better accuracy than original WRF observation-nudging method and WRF without nudging method.

Fig. 7 shows the contours of wind velocities at 2014_09_22_20:50:00 ~ 2014_09_22_22:20:00, at z = 54.5 m. The time increment is 30 min from left to right of each subgraph. As shown in Fig. 7, the wind field around the observation location can be greatly corrected by the observation-nudging method. At the bridge site, the wind blow into the valley between two mountains. However, in the simulation of WRF without nudging method, the diversion and acceleration effects of valley are not fully reflected. While in the original WRF observation-nudging simulation, although the observed wind velocity guides the simulation, but the influence is only dependent on the distance, i.e., the effects of observation data to the surrounding wind field is the same at the same distance from observation point. Therefore, the effect diffuses as a rigid disk moving. Obviously, it is unreasonable in the simulating the wind field over complex terrains. Because, as is well known, the natural wind is severely affected by the configuration of boundary layer, in the simulation of the spatial correlation-based observation-nudging approach, the wind field is clearly reflected the effect of the terrain and atmospheric circulation over time. From the perspective of wind field, it is true that the spatial correlation-based observation-nudging method is with more physical sense.

4. Wind characteristics based on spatial correlation-based WRF observation-nudging approach

From the wind field analysis in section 3, it can be seen clearly that the wind field obtained by spatial correlation-based observation-nudging method is more accurate and the physical sense is clearer. Therefore, the discussion in this section is mainly carried out under the spatial correlation-based observation-nudging method.

First, in Fig. 7(c), it exhibits obvious inhomogeneous characteristics of wind field along the bridge span, so that the bridge is subjected to an external load with spanwise characteristic, which is also the reason why the wind field surrounding the structure needs to be simulated accurately. Next, the wind field inhomogeneity is discussed in detail from the average wind characteristics along the bridge span, as shown in Fig. 8, where the four moments correspond to the above-mentioned flow field moments in Fig. 7.

Fig. 8(a) shows the average wind velocity. The effects of terrain and wind direction can be seen clearly from the average wind velocity in Fig. 8(a). During the time of 20:40~20:50, the wind comes from southeast direction, so the north side of bridge is dramatically affected by the mountain, indicating that the average velocity of north side of bridge is smaller than the south side. On the contrary, for the time interval of 21:10~21:20, 21:40~21:50 and 22:10~22:20, the wind comes from southwest direction, at these time intervals, the south side of bridge is remarkably affected by the mountain, and the average velocity is smaller than that at the north side. The influences of mountain from the magnitude comparison of average velocity between 1/4 central span and 3/4 central span in Fig. 8(a). Additionally, the average wind direction also presents remarkable inhomogeneity in Fig. 8(b).

In general, the local wind field shows a large extent of inhomogeneity under complex terrain surroundings.

5. Conclusions

In this paper a spatial correlation-based observation-nudging method to consider the multi-physical processes such as terrain and wind direction is proposed. Three simulation cases are conducted to analyze and compare the pros and cons of different methods, the comparison results show that the proposed spatial correlation-based observation-nudging method has obvious superiority for both the wind field and the single point wind velocity. Following conclusions can be obtained.

First, the validation test indicates that the average error of mean wind velocity obtained by spatial correlation-based observation-nudging method is dramatically improved, from -42.26% for the WRF without nudging method, -27.50% for the original WRF observation-nudging method, down to -7.13%. Furthermore, the results at other two locations also validate that the proposed method is much better than the original observation-nudging method and WRF without nudging method.

Then, from the perspective of wind field, the simulation results obtained by WRF without nudging method deviate greatly, which cannot fully reflect the influence of valley. For original observation-nudging method, the effect of observed value diffuses as a rigid disk moving, which is unreasonable in the simulating wind field over complex terrains. However, for the spatial correlation-based observation-nudging method, the wind field is clearly reflected the influence of the terrain and atmospheric circulation over time, which is more accuracy and physical sense.

Finally, by analyzing the wind field and average wind characteristics along the bridge span under spatial correlation-based observation-nudging method, it can observe that wind field exhibits obvious inhomogeneous characteristics along the bridge span, and it is reasonable and effective to consider the influence of the physical process such as terrain.

Acknowledgements

This study is financially supported by the National Key Research and Development Program of China under grant No. 2016YFC0701107, NSFC under grant Nos. 51508138, 51722805 and 51578188.

References

Bitsuamlak, G.T. and Abdi, D. (2016), "Wind flow simulations in idealized and real built environments with models of various level of complexity", *Wind Struct.*, **22**(4), 503-524.

Chen, F. and Dudhia, J. (2001), "Coupling an advanced land surface–hydrology model with the Penn State–NCAR MM5 modeling system. part I: model implementation and sensitivity", *Mon. Weather Rev.*, **129**, 569-585.

Cheng, X.L., Li, J., Hu, F., Xu, J. and Zhu, R. (2015), "Refined numerical simulation in wind resource assessment", *Wind Struct.*, **20**(1), 59-74.

Davis, C., Warner, T., Astling, E. and Bowers, J. (1999), "Development and application of an operational, relocatable, mesogamma scale weather analysis and forecasting system", *Tellus Series A-dynamic Meteorology & Oceanography*, **51**(5), 710-727.

Dhunny, A.Z., Lollchund, M.R. and Rughooputh, S.D. (2015), "A high-resolution mapping of wind energy potentials for Mauritius using Computational Fluid Dynamics (CFD)", *Wind Struct.*, **20**(4), 565-578.

Fast, J.D. (1995), "Mesoscale modeling and four-dimensional data assimilation in areas of highly complex terrain", *J. Appl. Meteor.*, **34**, 2762–2782.

Grell, G.A. and Freitas, S.R. (2014), "A scale and aerosol aware stochastic convective parameterization for weather and air quality modeling", *Atmosp. Chem. Phys.*, **14**(10), 5233-5250.

Hong, S., Dudhia, J. and Chen, S. (2004), "A revised approach to ice microphysical processes for the bulk parameterization of clouds and precipitation", *Mon. Weather Rev.*, **132**, 103-120.

Hong, S., Noh, Y. and Dudhia, J. (2006), "A new vertical diffusion package with an explicit treatment of entrainment processes", *Mon. Weather Rev.*, **134**, 2318-2341.

Iacono, M.J., Delamere, J.S., Mlawer, E.J., Shephard, M.W., Clough, S.A. and Collins, W.D. (2008), "Radiative forcing by long-lived greenhouse gases: calculations with the AER radiative transfer models", *J. Geophys. Res. Atmosp.*, **113**, **D13103.**

Leslie, L.M., LeMarshall, J.F., Morrison, R.P., Spinoso, C., Purser, R.J. and Pescod, N. (1998), "Improved hurricane track forecasting from the continuous assimilation of high-quality satellite wind data", *Mon. Weather Rev.*, **126**, 1248-1258.

Li, S.W., Hu, Z.Z., Tse, K.T. and Weerasuriya, A.U. (2016), "Wind direction field under the influence of topography: part II: CFD investigations", *Wind Struct.*, **22**(4), 477-501.

Liu, S., Pan, W., Zhang, H., Cheng, X., Long, Z. and Chen, Q. (2017), "CFD simulations of wind distribution in an urban community with a full-scale geometrical model", *Build. Environ.*, **117**, 11-23.

Liu, Y., Bourgeois, A., Warner, T., Swerdlin, S. and Hacker, J. (2005), "An implementation of obs-nudging-based FDDA into WRF for supporting ATEC test operations", *WRF/MM5 user's workshop*, Colorado, USA, June.

Liu, Y., Chen, F., Warner, T. and Basara, J. (2006), "Verification of a mesoscale data-assimilation and forecasting system for the Oklahoma City area during the joint urban 2003 field project", *J. Appl. Meteor.*, **45**(7), 912–929.

Liu, Y., Warner, T.T., Bowers, J.F., Carson, L.P., Chen, F. and Clough, C.A. (2008), "The operational mesogamma-scale analysis and forecast system of the U.S. Army test and evaluation command. part I: overview of the modeling system, the forecast products, and how the products are used", *J. Appl. Meteor.*, **47**(4), 1077-1092.

Liu, Y., Yu, W., Vandenberghe, F., Hahmann, F., Warner, A. and Swerdlin, S. (2006), "Assimilation of diverse meteorological datasets with a four-dimensional mesoscale analysis and forecast system", *Proceedings of the 10th Conference on Integrated Observing and Assimilation Systems for the Atmosphere, Oceans and Land Surface*, Atlanta, USA, January.

Liu, Y., Warner, T., Vincent, C., Wu, W. and Mahoney, B. (2011), "Simultaneous nested modeling from the synoptic scale to the LES scale for wind energy applications", *J. Wind Eng. Ind. Aerod.*, **99**(4), 308-319.

Mlawer, E., Taubman, S., Brown, P., Iacono, M. and Clough, S. (1997), "Radiative transfer for inhomogeneous atmospheres: RRTM, a validated correlated-k model for the longwave", *J. Geophys. Res.*, **102**(D14), 16 663-16 682.

Monti, P., Cantelli, A., Leuzzi, G., Valerio, G. and Pilotti, M. (2017), "Numerical simulations of mountain winds in an alpine valley", *Wind Struct.*, **24**(6), 565-578.

Pan, L.L., Chen, S.H., Dan, C., Lin, M.Y., Hart, Q. and Zhang, M.H. (2011), "Influences of climate change on California and Nevada regions revealed by a high-resolution dynamical downscaling study", *Clim. Dynam.*, 3**7**, 2005-2020.

Rife, D.L., Davis, C.A., Liu, Y. and Warner, T.T. (2004), "Predictability of low-level winds by mesoscale meteorological models", *Mon. Weather Rev.*, **132**(11), 2553-2569.

Rife, D.L., Warner, T.T., Chen, F. and Astling, E.G. (2002), "Mechanisms for diurnal boundary layer circulations in the Great Basin Desert", *Mon. Weather Rev.*, **130**(4), 921-938.

Seaman, N.L., Stauffer, D.R. and Lario-Gibbs, A.M. (1995), "A multiscale four-dimensional data assimilation system applied in the San Joaquin Valley during SARMAP. part I: modeling design and basic performance characteristics", *J. Appl. Meteor.*, **34**, 1739-1761.

Shen, L., Han, Y., Cai, C.S., Dong, G., Zhang, J. and Hu, P. (2017), "LES of wind environments in urban residential areas based on an inflow turbulence generating approach", *Wind Struct.*, **24**(1), 1-24.

Skamarock, W.C., Klemp, J.B., Dudhia, J., Gill, D.O., Barker, D.M. and Duda, M. (2008), "A description of the advanced research WRF version 3", *NCAR Technical*, **113**, 7-25.

Stauffer, D.R. and Seaman, N.L. (1994), "Multiscale four-dimensional data assimilation", *J. Appl. Meteor.*, **33**, 416-434.

Warner, T.T., Bowers, J.F., Swerdlin, S.P. and Beitler, B.A. (2004), "A rapidly deployable operational mesoscale modeling system for emergency-response applications", *Bull. Am. Meteorol. Soc.*, **85**(5), 709-716.

Weerasuriya, A.U., Hu, Z.Z., Li, S.W. and Tse, K.T. (2016), "Wind direction field under the influence of topography, part I: a descriptive model", *Wind Struct.*, **22**(4), 455-476.

Xu, M., Liu, Y., Davis, C.A. and Warner, T.T. (2002), "Sensitivity study on nudging parameters for a mesoscale FDDA system". *Proceedings of the 19th Conference on Weather Analysis and Forecasting/15th Conference on Numerical Weather Prediction*, San Antonio, USA, July.

Zajaczkowski, F.J., Haupt, S.E. and Schmehl, K.J. (2011), "A preliminary study of assimilating numerical weather prediction data into computational fluid dynamics models for wind prediction", *J. Wind Eng. Ind. Aerod.*, **99**(4), 320-329.

Zhang, Y., Liu, Y. and Nipen, T. (2016), "Evaluation of the impacts of assimilating the TAMDAR data on 12/4 km grid WRF-based RTFDDA simulations over the CONUS", **2016**, 1-13.

CC